Improved measurement of the semileptonic decay $D_s^+ \to K^0 e^+ \nu_e$

M. Ablikim *et al.*[*]
(BESIII Collaboration)

(Received 27 June 2024; accepted 4 September 2024; published 30 September 2024)

Analyzing e^+e^- collision data corresponding to an integrated luminosity of 7.33 fb^{-1} collected at center-of-mass energies between 4.128 and 4.226 GeV with the BESIII detector, we measure the branching fraction of the semileptonic decay $D_s^+ \to K^0 e^+ \nu_e$ to be $(2.98 \pm 0.23_{\mathrm{stat}} \pm 0.12_{\mathrm{syst}}) \times 10^{-3}$. Based on fit to the partial decay rates in various q^2 intervals, the product value of $D_s^+ \to K^0$ hadronic form factor and Cabibbo-Kobayashi-Maskawa element is measured to be $f_+^{K^0}(0)|V_{cd}| = 0.143 \pm 0.011_{\mathrm{stat}} \pm 0.003_{\mathrm{syst}}$. With $|V_{cd}| = 0.22486 \pm 0.00067$ as an input, the hadronic form factor is evaluated to be $f_+^{K^0}(0) = 0.636 \pm 0.049_{\mathrm{stat}} \pm 0.013_{\mathrm{syst}}$. The branching fraction and form factor measurements are factors of 1.6 and 1.7 more precise than the previous world averages, respectively.

DOI: 10.1103/PhysRevD.110.052012

I. INTRODUCTION

Studies of semileptonic D_s^+ decays provide important input to understand the effects of the strong and weak interactions in charmed meson decays [1]. The partial decay rates of the semileptonic decays $D_s^+ \to P \ell^+ \nu_\ell$ (P denotes a pseudoscalar meson) are proportional to the product of the hadronic form factor $f_+^P(0)$ and the Cabibbo-Kobayashi-Maskawa (CKM) matrix element $|V_{cs}|$ or $|V_{cd}|$. In recent years, there has been much progress in the experimental study of semileptonic D_s^+ decays. However, knowledge of Cabibbo-suppressed semileptonic D_s^+ decays remains limited by statistical uncertainty [2]. Improved measurements of the branching fraction of $D_s^+ \to K^0 e^+ \nu_e$ and the hadronic form factor of $D_s^+ \to K^0$ are important to validate theoretical calculations [3–11]. The hadronic form factor measurement helps test and improve theoretical calculations, which in turn improves the measured precision of $|V_{cd}|$. This is important for testing the unitary of the CKM matrix and searching for possible indications of new physics.

Theoretical predictions of the branching fraction of $D_s^+ \to K^0 e^+ \nu_e$ range from 2.0×10^{-3} to 4.0×10^{-3}. In 2009, the CLEO-c experiment reported the first measurement of the branching fraction of $D_s^+ \to K^0 e^+ \nu_e$ using 0.31 fb^{-1} of e^+e^- collision data collected at a c.m. energy of 4.17 GeV [12]. In 2015, the CLEO collaboration updated the branching fraction measurement using 0.586 fb^{-1} of data at the same energy point [13]. In 2019, the BESIII experiment presented a further improved measurement of the branching fraction and the first measurement of the hadronic form factor in $D_s^+ \to K^0 e^+ \nu_e$ by analyzing 3.19 fb^{-1} of data at 4.178 GeV [14,15].

In this paper, we report improved measurements of both the branching fraction and the hadronic transition form factor in $D_s^+ \to K^0 e^+ \nu_e$, where the K^0 is reconstructed as K_S^0 assuming that K_S^0 accounts for 50% of the magnitude and neglecting the CP violation effects in neutral kaon decay. The measurement is performed based on 7.33 fb^{-1} of e^+e^- collision data taken with c.m. energies between 4.128 and 4.226 GeV with the BESIII detector. The c.m. energies for each of the datasets are summarized in the Table I. Throughout this paper, charge conjugate modes are implied.

TABLE I. The c.m. energies and M_{BC} requirements for various datasets.

Dataset	$E_{\mathrm{c.m.}}$ (GeV)	M_{BC} (GeV/c^2)
1	4.128	[2.010, 2.061]
2	4.157	[2.010, 2.070]
3	4.178	[2.010, 2.073]
4	4.189	[2.010, 2.076]
5	4.199	[2.010, 2.079]
6	4.209	[2.010, 2.082]
7	4.219	[2.010, 2.085]
8	4.226	[2.010, 2.088]

[*]Full author list given at the end of the article.

II. BESIII DETECTOR AND MONTE CARLO SIMULATIONS

The BESIII detector [16] records symmetric e^+e^- collisions provided by the BEPCII storage ring [17], which operates with a peak luminosity of 1.1×10^{33} cm^{-2} s^{-1} in the c.m. energy range from 1.84 to 4.95 GeV. BESIII has collected large data samples in this energy region [18]. The cylindrical core of the BESIII detector covers 93% of the full solid angle and consists of a helium-based multilayer drift chamber (MDC), a plastic scintillator time-of-flight system (TOF), and a CsI(Tl) electromagnetic calorimeter (EMC), all enclosed in a superconducting solenoidal magnet that provides a 1.0 T magnetic field. The solenoid is supported by an octagonal flux-return yoke with resistive plate counter muon identification modules interleaved with steel. The charged-particle momentum resolution at 1 GeV/c is 0.5%, and the dE/dx resolution is 6% for electrons from Bhabha scattering. The EMC measures photon energies with a resolution of 2.5% (5%) at 1 GeV in the barrel (end cap) region. The time resolution in the TOF barrel (end cap) region is 68 (110) ps, and the end cap TOF system was upgraded in 2015 using multi-gap resistive plate chamber technology, providing a time resolution of 60 ps [19]. Approximately 83% of the data benefits from this upgrade.

Simulated data samples produced with a Geant4-based [20] Monte Carlo (MC) package, which includes the geometric description of the BESIII detector and the detector response, are used to determine detection efficiencies and to estimate backgrounds. The simulation models the beam energy spread and initial state radiation in the e^+e^- annihilations with the generator KKMC [21]. In the simulation, the production of open-charm processes directly produced via e^+e^- annihilations are modeled with the generator CONEXC [22], and their subsequent decays are modeled by EvtGen [23] with known branching fractions from the Particle Data Group (PDG) [2]. The initial state radiation production of vector charmonium (like) states and the continuum processes are incorporated in KKMC [21]. The remaining unknown charmonium decays are modeled with LUNDCHARM [24]. Final state radiation from charged final-state particles is incorporated using the PHOTOS package [25].

III. ANALYSIS METHOD

Pairs of $D_s^{*\pm}D_s^{\mp}$ decaying into $\gamma D_s^+ D_s^-$ are produced copiously in e^+e^- collisions with c.m. energies between 4.128 and 4.226 GeV. This allows us to study D_s^+ decays using the double-tag (DT) method pioneered by the MARK-III collaboration [26]. The D_s^- meson, which is fully reconstructed via one of its hadronic decay modes, is referred to as a single-tag (ST) D_s^- meson. In the presence of a fully reconstructed ST D_s^- meson at a certain c.m. energy, we can infer the kinematic information of the other D_s^+ meson. The semileptonic decay $D_s^+ \to K^0 e^+ \nu$ is thus selected on the side recoiling against the ST D_s^-, despite the presence of an undetectable neutrino. A DT event is an event in which the transition γ from the D_s^{*+} and the semileptonic decay $D_s^+ \to K^0 e^+ \nu_e$ can be successfully selected in the presence of the ST. The branching fraction of $D_s^+ \to K^0 e^+ \nu_e$ is determined by

$$\mathcal{B}_{D_s^+ \to K^0 e^+ \nu_e} = \frac{N_{\rm DT}}{N_{\rm ST}^{\rm tot} \cdot \bar{\epsilon}_{\gamma \rm SL}}, \tag{1}$$

where $N_{\rm DT} = \sum_{ij} N_{\rm DT}^{ij}$ and $N_{\rm ST}^{\rm tot} = \sum_{ij} N_{\rm ST}^{ij}$ are the yields of the DT events and ST D_s^- mesons in data summing over all tag modes i and datasets j, respectively; and $\bar{\epsilon}_{\gamma \rm SL}$ is the efficiency of detecting the γ and the semileptonic decay in the presence of the ST D_s^- candidate, weighted by the ST yield in data. It is calculated by $\sum_{ij}[(N_{\rm ST}^{ij}/N_{\rm ST}) \cdot (\epsilon_{\rm DT}^{ij}/\epsilon_{\rm ST}^{ij})]$, where $\epsilon_{\rm DT}^{ij}$ and $\epsilon_{\rm ST}^{ij}$ are the detection efficiencies of the DT and ST candidates, respectively.

IV. SINGLE-TAG D_s^- CANDIDATES

The ST D_s^- candidates are formed using 14 hadronic decay modes: $D_s^- \to K^+K^-\pi^-$, $K^+K^-\pi^-\pi^0$, $\pi^+\pi^-\pi^-$, $K_S^0K^-$, $K_S^0K^-\pi^0$,$K^-\pi^+\pi^-$, $K_S^0K_S^0\pi^-$, $K_S^0K^+\pi^-\pi^-$, $K_S^0K^-\pi^+\pi^-$, $\eta_{\gamma\gamma}\pi^-$, $\eta'_{\pi^+\pi^-\eta}\rho^-$, $\eta'_{\eta_{\gamma\gamma}\pi^+\pi^-}\pi^-$, $\eta'_{\gamma\rho^0}\pi^-$, and $\eta_{\gamma\gamma}\rho^-$. Throughout this paper, the subscripts on the $\eta^{(\prime)}$ denote the decay modes that are used to reconstruct the $\eta^{(\prime)}$ candidates and ρ denotes $\rho(770)$.

In selecting candidates for the $K^\pm$, $\pi^\pm$, K_S^0, γ, π^0, and η, we use the same selection criteria as those adopted in our previous works [27,28]. All charged tracks, except for those from K_S^0 decays, are required to originate from the interaction point (IP) defined by $|V_{xy}| < 1$ cm, $|V_z| < 10$ cm, and $|\cos\theta| < 0.93$ to ensure reliable main drift chamber measurements, where $|V_{xy}|$ and $|V_z|$ are the distances of closest approach to the IP in the transverse plane and along the MDC axis, respectively, and θ is the polar angle with respect to the MDC axis. The particle identification (PID) of charged particles is performed with combined dE/dx and TOF information. Those with confidence level for the pion (kaon) hypothesis greater than that for the kaon (pion) hypothesis are assigned to be pion (kaon) candidates.

Candidates for K_S^0 are reconstructed from two oppositely charged tracks satisfying $|V_z| < 20$ cm because of the long lifetime of the K_S^0 meson. The two charged tracks are assigned as $\pi^+\pi^-$ without imposing further PID criteria. They are constrained to originate from a common vertex and are required to have an invariant mass within $|M_{\pi^+\pi^-} - m_{K_S^0}| < 12$ MeV/c^2, where $m_{K_S^0}$ is the K_S^0 nominal mass [2]. The decay length of the K_S^0 candidate is required to be greater than twice the vertex resolution away from the IP to suppress the combinatorial backgrounds of $\pi^+\pi^-$ originated from the non-K_S^0 decay.

Photon candidates are selected using information measured by the EMC and are required to satisfy the following criteria. To suppress backgrounds from electronic noise or bremsstrahlung, any candidate shower is required to start within [0, 700] ns from the event start time. The energy of each shower in the barrel (end cap) region of the EMC [16] is required to be greater than 25 (50) MeV. To suppress backgrounds associated with charged tracks, the minimum opening angle between the momentum of the candidate shower and the extrapolated momentum direction of the nearest charged track at the EMC has to be greater than 10°.

Candidates for π^0 and $\eta_{\gamma\gamma}$ are formed from $\gamma\gamma$ pairs with invariant masses in the mass intervals (0.115, 0.150) and $(0.50, 0.57)$ GeV/c^2, respectively. To improve momentum resolution, the invariant mass of each selected $\gamma\gamma$ pair is constrained to either the π^0 or η nominal mass [2]. To form candidates for $\rho^{0(+)}$, $\eta_{\pi^0\pi^+\pi^-}$, $\eta'_{\eta\pi^+\pi^-}$, and $\eta'_{\gamma\rho^0}$, the invariant masses of the $\pi^+\pi^{-(0)}$, $\pi^0\pi^+\pi^-$, $\eta\pi^+\pi^-$, and $\gamma\rho^0$ combinations are required to be within the mass intervals of (0.57, 0.97), (0.53, 0.57), (0.946, 0.970), and $(0.940, 0.976)$ GeV/c^2, respectively. These mass intervals correspond to approximately ± 3 times of the standard deviations around the peaks of the reconstructed particles. In addition, to suppress the backgrounds from D^* decays, the momenta of the photon from $\eta' \to \gamma\rho$ and all pions are required to be greater than 0.1 GeV/c.

The backgrounds from non-$D_s^{\pm}D_s^{*\mp}$ processes are suppressed with the beam-constrained mass of the ST D_s^- candidate, which is defined as

$$M_{\rm BC} \equiv \sqrt{E_{\rm beam}^2/c^4 - |\vec{p}_{\rm tag}|^2/c^2}, \tag{2}$$

where $E_{\rm beam}$ is the beam energy and $\vec{p}_{\rm tag}$ is the momentum of the ST D_s^- candidate in the e^+e^- c.m. frame. The $M_{\rm BC}$ is required to be within the intervals shown in Table I. This requirement retains 90% of the D_s^- and D_s^+ mesons from $e^+e^- \to D_s^{*\mp}D_s^{\pm}$.

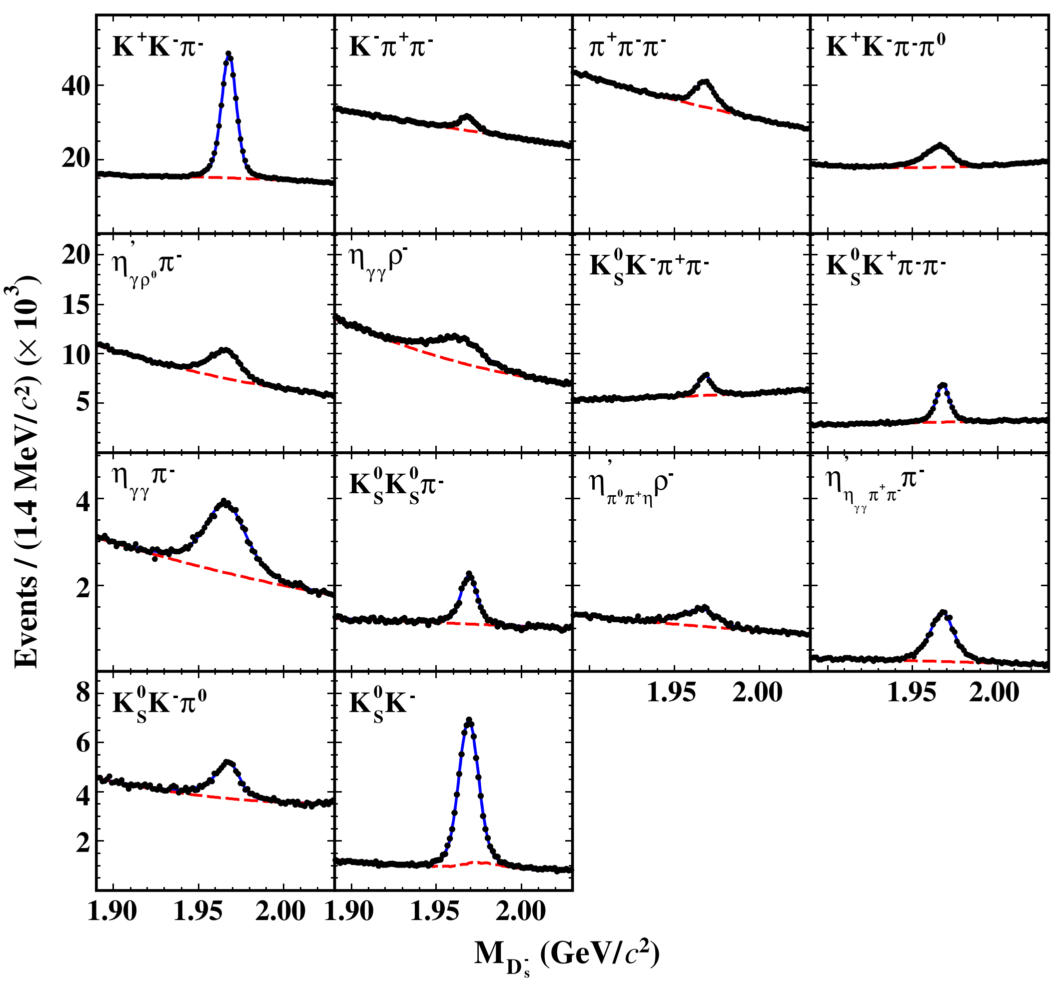

FIG. 1. Fits to the $M_{D_s^-}$ distributions of the ST candidates for various tag modes. The points with error bars are data; the blue solid curves are the best fit results; and the red dashed curves are the fitted background shapes.

In the case of multiple candidates, only the candidate with the D_s^- recoil mass

$$M_{\rm rec} \equiv \sqrt{\left(E_{\rm c.m.}/c^2 - \sqrt{|\vec{p}_{\rm tag}|^2/c^2 + m_{D_s^-}^2}\right)^2 - |\vec{p}_{\rm tag}|^2/c^2} \quad (3)$$

closest to the D_s^{*+} nominal mass [2] per tag mode is retained for further analysis. The distributions of the invariant mass ($M_{\rm tag}$) of the accepted ST candidates for various tag modes are shown in Fig. 1. The yields of ST D_s^- mesons reconstructed in various tag modes are derived from fits to individual $M_{\rm tag}$ distributions and are listed in Table II. In the fits, the signals are described by the simulated signal shapes convolved with Gaussian functions to incorporate the possible resolution differences between data and simulation, where the widths of the convolved Gaussian functions range from (0.6 ± 0.2) MeV$/c^2$ to (3.5 ± 1.3) MeV$/c^2$ for different ST modes. The combinatorial background is described by a second-order Chebychev polynomial function and has been verified with the inclusive MC sample. For the $D_s^- \to K_S^0 K^-$ tag, the broad peaking background from $D^- \to K_S^0 \pi^-$ is modeled using the simulated shape and the size of this background relative to other combinatorial ones is fixed. Figure 1 shows the results of the fit to the data sample. For each tag mode, the ST yield is obtained by integrating the signal shape over the selected D_s^- signal region defined within $1.94 < M_{D_s^-} < 1.99$ GeV$/c^2$. The second and third columns of Table II summarize the yields of ST D_s^- mesons ($N_{\rm ST}$) for various tag modes obtained from the data sample and the corresponding detection efficiencies ($\epsilon_{\rm ST}$), respectively. The total ST yield summed over all ST modes is $N_{\rm ST}^{\rm tot} = (783.1 \pm 2.5) \times 10^{-3}$, where the uncertainty is statistical only.

V. SELECTION OF $D_s^+ \to K^0 e^+ \nu_e$

In the system recoiling against the D_s^- tag and the transition γ from the D_s^{*-}, the semileptonic decay $D_s^+ \to K^0 e^+ \nu_e$ is selected using tracks that have not been used for the single tag reconstruction. To identify positrons, the combined confidence levels CL'_e, CL'_π, and CL'_K for the electron, pion, and kaon hypotheses are calculated with the d$E/$dx, TOF, and EMC information. The positron candidates are required to satisfy $CL'_e > 0.001$ and $CL'_e/(CL'_e + CL'_\pi + CL'_K) > 0.8$.

Due to the misidentifications between charged kaons and positrons, the background from $D_s^+ \to K^0 K^+$ can be reconstructed as $D_s^+ \to K^0 e^+ \nu_e$. This background is vetoed by requiring the invariant mass of $K^0 e^+$ to be less than 1.78 GeV$/c^2$. The background contributions from D_s^+ hadronic decays associated with fake photons misidentified from showers are rejected by requiring the largest energy of the unused showers ($E_{{\rm extra}\gamma}^{\rm max}$) to be less than 0.2 GeV. The DT candidate is rejected if additional charged tracks ($N_{\rm extra}^{\rm charge}$) is detected.

To identify the transition γ produced directly from the $D_s^{*\pm}$, we perform kinematic fits under two hypotheses. One assumes that the D_s^{*-} is formed by the transition γ and the ST D_s^-, and the other assumes that the D_s^{*+} is formed by the transition γ and the semileptonic decay. The final particles from the $D_s^{\mp} D_s^{*\pm}$ system are constrained to obey energy and momentum conservation in the e^+e^- c.m. frame with the neutrino treated as a missing particle. The particle candidates for $D_s^{\pm}$ are constrained to their known mass from the PDG [2]. For the former hypothesis, the mass of the transition γ and the tagged D_s^- is constrained to the known D_s^{*-} mass. For the latter hypothesis, the mass of the transition γ and the semileptonic decay is constrained to the known D_s^{*+} mass. The hypothesis with the smallest χ^2 of the kinematic fit ($\chi^2_{\rm KMFIT}$), which also satisfies $\chi^2_{\rm KMFIT} < 100$, is kept for further analysis.

The presence of the neutrino is inferred from the distribution of the missing-mass squared variable, which is defined as

$$M_{\rm miss}^2 = E_{\rm miss}^2/c^4 - |\vec{p}_{\rm miss}|^2/c^2. \quad (4)$$

Here, $E_{\rm miss} = E_{\rm c.m.} - \Sigma_i E_i$ and $\vec{p}_{\rm miss} = \Sigma_i \vec{p}_i$, where E_i and $\vec{p}_i$, with $i =$ (tag, γ, e, and K^0), are the energy and momentum of particle i.

The $M_{\rm miss}^2$ distribution of the accepted candidates for $D_s^+ \to K^0 e^+ \nu_e$ in data summed over all c.m. energies is shown in Fig. 2. The signal yield of $D_s^+ \to K^0 e^+ \nu_e (N_{\rm DT})$ is

TABLE II. Fitted yields of single-tag D_s^- mesons from the data sample ($N_{\rm ST}$), the efficiencies of detecting single-tag D_s^- mesons and double-tag events ($\epsilon_{\rm ST}$ and $\epsilon_{\rm DT}$) for various tag modes. For all quantities, the uncertainties are statistical only. The listed efficiencies do not include the branching fractions of the daughter particles's decays.

Tag mode	$N_{\rm ST}$ ($\times 10^3$)	$\epsilon_{\rm ST}$ (%)	$\epsilon_{\rm DT}$ (%)
$K^+K^-\pi^-$	281.7 ± 0.8	41.94 ± 0.03	10.92 ± 0.11
$K^+K^-\pi^-\pi^0$	85.4 ± 1.0	11.53 ± 0.03	3.39 ± 0.12
$\pi^-\pi^+\pi^-$	76.9 ± 1.0	53.84 ± 0.06	15.28 ± 0.11
$K_S^0 K^-$	63.2 ± 0.3	47.18 ± 0.06	12.73 ± 0.11
$K_S^0 K^-\pi^0$	21.9 ± 0.5	16.56 ± 0.08	4.81 ± 0.12
$K^-\pi^+\pi^-$	36.8 ± 0.8	47.06 ± 0.08	12.78 ± 0.11
$K_S^0 K_S^0 \pi^-$	10.6 ± 0.2	22.92 ± 0.13	5.82 ± 0.12
$K_S^0 K^+\pi^-\pi^-$	30.5 ± 0.3	21.48 ± 0.07	5.48 ± 0.12
$K_S^0 K^-\pi^+\pi^-$	16.4 ± 0.4	19.21 ± 0.10	4.74 ± 0.12
$\eta\pi^-$	33.7 ± 0.6	40.43 ± 0.08	12.54 ± 0.11
$\eta'(\pi^+\pi^-\eta)\rho^-$	7.2 ± 0.3	5.62 ± 0.08	1.83 ± 0.11
$\eta'(\eta\pi^+\pi^-)\pi^-$	15.6 ± 0.2	19.20 ± 0.10	5.45 ± 0.12
$\eta'(\gamma\rho)\pi^-$	47.3 ± 0.7	30.94 ± 0.07	8.77 ± 0.11
$\eta\rho^-$	56.0 ± 1.2	14.35 ± 0.04	5.02 ± 0.12

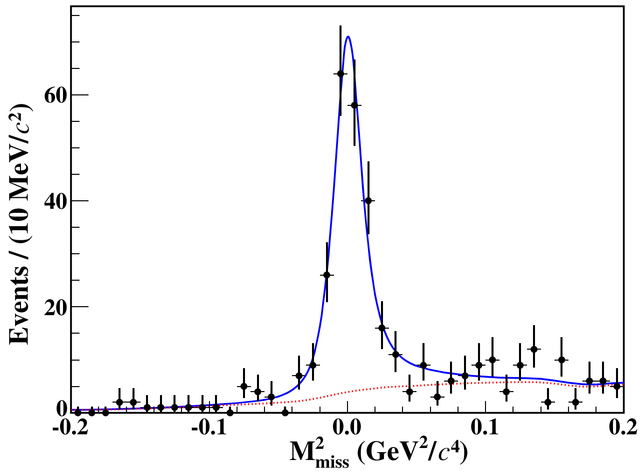

FIG. 2. Fit to the $M^2_{\rm miss}$ distribution of the candidates for $D_s^+ \to K^0 e^+ \nu_e$. The points with error bars are the data summed over all c.m. energies, the blue solid curve is the total fit, and the red dashed curve is the fitted background shape.

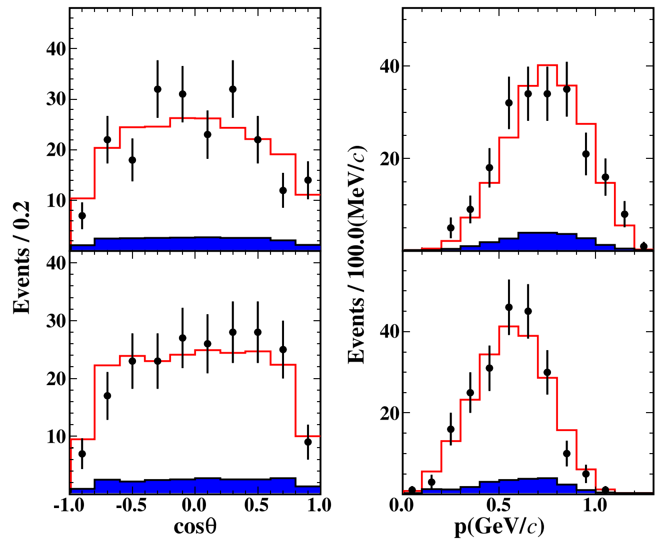

FIG. 3. Comparison of $\cos\theta$ and momenta for the K^0 (top) and candidates for $D_s^+ \to K^0 e^+ \nu_e$ (bottom) using all c.m. energies between 4.128 and 4.226 GeV. The points with error bars are data, the blue filled histograms are the simulated background, and the red line histograms are the inclusive MC samples. These events have been required to satisfy $|M^2_{\rm miss}| < 0.03$ GeV$^2/c^4$.

derived from an unbinned maximum likelihood fit to this distribution. In this fit, the signal is described by a simulated signal shape convolved with a Gaussian function, where the width of the Gaussian function is $(0.5 \pm 0.3) \times 10^{-3}$ GeV$^2/c^4$ determined from the fit. The background is described by a simulated shape derived from the inclusive MC sample. From this fit, the signal yield is 225.3 ± 17.3 where the uncertainty is statistical only. The corresponding DT efficiencies $\epsilon^i_{\rm DT}$ of various ST are summarized in the fourth column of Table II.

VI. BRANCHING FRACTION

The detection efficiency $\varepsilon_{\rm SL}$, which does not include the branching fraction of $K^0 \to K^0_S \to \pi^+\pi^-$, is estimated to be $(27.88 \pm 0.21)\%$ for $D_s^+ \to K^0 e^+ \nu_e$. Figure 3 shows good consistency in the $\cos\theta$ and momenta distributions for the K^0 and $D_s^+ \to K^0 e^+ \nu_e$ candidates between data and the inclusive MC sample. The branching fraction of $D_s^+ \to K^0 e^+ \nu_e$ is determined by Eq. (1) to be

$$\mathcal{B}(D_s^+ \to K^0 e^+ \nu_e) = (2.98 \pm 0.23 \pm 0.12) \times 10^{-3},$$

where the first uncertainty is statistical and the second is systematic, which is discussed below and summarized in Table III.

Our measurement is performed using the DT technique [26], and most systematic uncertainties related to the ST selection criteria therefore cancel. The systematic uncertainty of the ST D_s^- yields is evaluated to be 1.0% by using alternative signal and background shapes in the fits to the $M_{\rm tag}$ spectra. The systematic uncertainty for the $e^\pm$ tracking and PID efficiency is 1.0% each and is studied using a control sample of $e^+e^- \to \gamma e^+ e^-$ [29]. The systematic uncertainty in the K^0_S reconstruction efficiency is estimated with the control samples $J/\psi \to K^*(892)^\mp K^\pm$ and $J/\psi \to \phi K^0_S K^\pm \pi^\mp$ [30] and is determined to be 1.5% per K^0_S. The systematic uncertainty of the transition γ reconstruction [31], which is weighted by the branching fraction of $D_s^{*+} \to \gamma D_s^+$, is assigned to be 1.0%. For requirements on $E^{\rm max}_{{\rm extra}\gamma}$ and $N^{\rm charge}_{\rm extra}$ and $\chi^2_{\rm KMFIT}$, their systematic uncertainties are studied using control samples $D_s^+ \to K^0_S K^+$ and $D_s^+ \to K^0_S K^+ \pi^0$, where the accepted efficiencies of the $E^{\rm max}_{{\rm extra}\gamma}$, $N^{\rm charge}_{\rm extra}$, and $\chi^2_{\rm KMFIT}$ requirements are evaluated for both data and MC samples. Then the differences of the accepted efficiencies between data and MC samples, 0.8% for $E^{\rm max}_{{\rm extra}\gamma}$ and $N^{\rm charge}_{\rm extra}$ and 2.3% for $\chi^2_{\rm KMFIT}$, are assigned as their systematic uncertainties. The systematic uncertainty due to the different tag dependence between data and MC simulation, called the tag bias [29], is estimated to be 0.2%. The systematic uncertainty due to the quoted branching fraction of $K^0 \to K^0_S \to \pi^+\pi^-$ is evaluated as 0.2% [2], which incorporates a 0.2% uncertainty because of the negligence of the possible CP violations in neutron kaon decays. The systematic uncertainty arising from the fit to the $M^2_{\rm miss}$ distribution is estimated to be 0.9% by varying the signal and background shapes. The uncertainty due to MC statistics is 0.2%. Systematic uncertainty due to the uncertainty on the form factor used in the MC simulation to determine the efficiency is estimated to be 1.4%. This is evaluated by comparing the difference of the signal efficiencies when varying the input hadronic form factor parameter by $\pm 1\sigma$, as determined in this work listed in Table VIII. Adding these effects in quadrature, we obtain

TABLE III. Sources of systematic uncertainties in the branching fraction measurement.

Source	Uncertainty (%)
Single-tag yield	1.0
e^+ tracking	1.0
e^+ PID	1.0
K_S^0 reconstruction	1.5
Transition γ reconstruction	1.0
$E_{\mathrm{extra}\gamma}^{\mathrm{max}}$ and $N_{\mathrm{extra}}^{\mathrm{charge}}$ requirements	0.8
χ^2_{KMFIT} requirement	2.3
Tag bias	0.2
Quoted branching fraction	0.2
M^2_{miss} fit	0.9
MC statistics	0.2
Hadronic form factor	1.4
Total	3.9

the total systematic uncertainty on the measurement of the branching fraction of $D_s^+ \to K^0 e^+ \nu_e$ to be 3.9%. A summary of the systematic uncertainties for the branching fraction is shown in Table III.

VII. HADRONIC FORM FACTOR

To study the decay dynamics of the semileptonic decay $D_s^+ \to K^0 e^+ \nu_e$, candidates are divided according to the invariant mass squared of the $e^+\nu_e$ system ($q^2 = (E_e/c + E_\nu/c)^2 + |\vec{p}_e + \vec{p}_\nu|^2$) into five intervals (0.00, 0.35], (0.35, 0.70], (0.70, 1.05], (1.05, 1.40], and (1.40, 2.16) GeV^2/c^4. The partial decay rate in the ith q^2 interval, $\Delta\Gamma^i_{\mathrm{measured}}$, is determined by

$$\Delta\Gamma^i_{\mathrm{measured}} = N^i_{\mathrm{produced}}/(\tau_{D_s^+}\mathcal{B}_{K^0\to\pi^+\pi^-}N^{\mathrm{tot}}_{\mathrm{ST}}), \quad (5)$$

where N^i_{produced} is the $D_s^+ \to K^0 e^+ \nu_e$ signal yield produced in the ith q^2 interval in data, $\tau_{D_s^+}$ is the lifetime of the D_s^+ [2], and $N^{\mathrm{tot}}_{\mathrm{ST}}$ is the total yield of ST D_s^- mesons. The number of events produced in data is calculated as

$$N^i_{\mathrm{produced}} = \sum_j^{N_{\mathrm{intervals}}} (\varepsilon^{-1})_{ij} N^j_{\mathrm{observed}}, \quad (6)$$

where N^j_{observed} is the $D_s^+ \to K^0 e^+ \nu_e$ signal yield observed in the jth q^2 interval and ε is the efficiency matrix, which also includes the effects of bin migration, given by

$$\varepsilon_{ij} = \sum_k [(N^{ij}_{\mathrm{reconstructed}} \cdot N_{\mathrm{ST}})/(N^j_{\mathrm{generated}} \cdot \varepsilon_{\mathrm{ST}})]_k / N^{\mathrm{tot}}_{\mathrm{ST}}. \quad (7)$$

Here, $N^{ij}_{\mathrm{reconstructed}}$ is the $D_s^+ \to K^0 e^+ \nu_e$ signal yield generated in the jth q^2 interval and reconstructed in the ith q^2 interval, $N^j_{\mathrm{generated}}$ is the total signal yield generated in the jth q^2 interval, and the index k sums over all tag modes and energies.

The signal yield N^i_{observed} in each q^2 interval is obtained from the fit to the corresponding M^2_{miss} distribution, and is shown in Fig. 4. The efficiency matrix for $D_s^+ \to K^0 e^+ \nu_e$ is

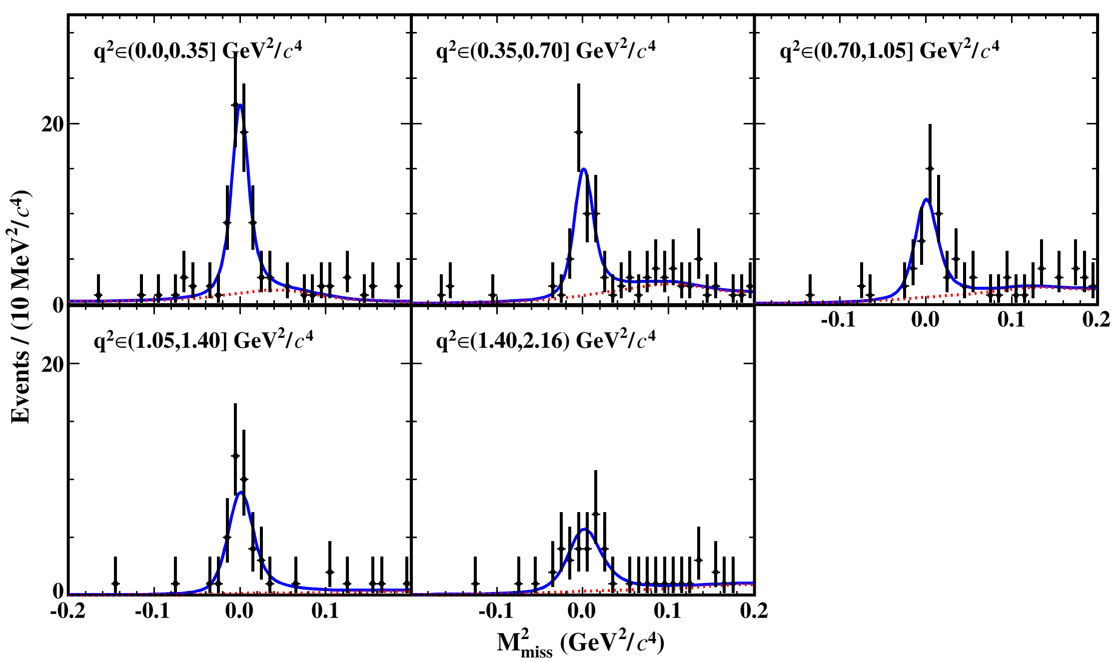

FIG. 4. Fits to the M^2_{miss} distributions of $D_s^+ \to K^0 e^+ \nu_e$ in various reconstructed q^2 intervals. The points with error bars are the data summed over all c.m. energies, the blue solid curves are the best fits, and the red dashed curves are the fitted background shapes.

TABLE IV. Efficiency matrix (in %) for $D_s^+ \to K^0 e^+ \nu_e$. The efficiencies do not include the branching fractions of the decays of the daughter particles.

$(i,j) q^2$ interval	1	2	3	4	5
1	26.80	0.83	0.00	0.00	0.00
2	0.93	27.62	0.74	0.02	0.00
3	0.00	0.91	27.09	0.64	0.00
4	0.00	0.00	0.83	26.12	0.41
5	0.00	0.00	0.00	0.70	25.56

shown in Table IV. The values for $N^j_{\rm observed}$, $N^j_{\rm produced}$, $\Delta\Gamma_j$, and $\frac{\Delta\Gamma_j}{\Delta q^2_j}$ are summarized in Table V.

Using the values of $\Delta\Gamma^i_{\rm measured}$ obtained above and the theoretical parametrization of the partial decay rate $\Delta\Gamma^i_{\rm expected}$ described below, form factor parameters are extracted by a χ^2 fit where the χ^2 is constructed as

$$\chi^2 = \sum_{i,j=1}^{5} (\Delta\Gamma^i_{\rm measured} - \Delta\Gamma^i_{\rm expected}) C^{-1}_{ij} \times (\Delta\Gamma^j_{\rm measured} - \Delta\Gamma^j_{\rm expected}), \quad (8)$$

where $C_{ij} = C^{\rm stat}_{ij} + C^{\rm syst}_{ij}$ is the covariance matrix of the measured partial decay rates among q^2 intervals. The differential decay rate is given by

$$\frac{d\Gamma(D_s^+ \to K^0 e^+ \nu_e)}{dq^2} = \frac{G_F^2 |V_{cd}|^2}{24\pi^3} p^3_{K^0} |f_+^{K^0}(q^2)|^2, \quad (9)$$

where p_{K^0} is the K^0 momentum in the rest frame of the D_s^+, G_F is the Fermi coupling constant [2], $|V_{cd}|$ is the $c \to d$ CKM matrix element, and $f_+^{K^0}(q^2)$ is the hadronic form factor. The scalar hadronic form factor $f_0^{K^0}(q^2)$ has been ignored because it is proportional to the positron mass squared.

The hadronic form factor, $f_+^{K^0}(q^2)$, is usually parametrized by the simple pole model, modified pole model, or series expansion. In the modified pole model [32],

TABLE VI. The statistical correlation coefficients of the measured partial decay rate in each q^2 bin for $D_s^+ \to K^0 e^+ \nu_e$.

ϵ_{ij}	1	2	3	4	5
1	1.000	−0.065	0.003	−0.000	0.000
2	−0.065	1.000	−0.060	0.003	−0.000
3	0.003	−0.060	1.000	−0.057	0.002
4	−0.000	0.003	−0.057	1.000	−0.044
5	0.000	−0.000	0.020	−0.044	1.000

TABLE VII. The systematic correlation coefficients of the measured partial decay rate in each q^2 bin for $D_s^+ \to K^0 e^+ \nu_e$.

ϵ_{ij}	1	2	3	4	5
1	1.000	0.920	0.814	0.952	0.590
2	0.920	1.000	0.816	0.844	0.706
3	0.814	0.816	1.000	0.782	0.893
4	0.952	0.844	0.782	1.000	0.519
5	0.590	0.706	0.893	0.519	1.000

$$f_+^{K^0}(q^2) = \frac{f_+^{K^0}(0)}{\left(1 - \frac{q^2}{M^2_{\rm pole}}\right)\left(1 - \alpha \frac{q^2}{M^2_{\rm pole}}\right)}, \quad (10)$$

where $M_{\rm pole}$ is fixed to the known D^{*+} mass and α is a free parameter. Setting $\alpha = 0$ and leaving $M_{\rm pole}$ free, the simple pole model is recovered [33]. Due to limited statistics, we adopt the two parameter series expansion form, which is written as

$$f_+^{K^0}(q^2) = \frac{f_+^{K^0}(0) P(0) \Phi(0, t_0)}{P(q^2) \Phi(q^2, t_0)} \cdot \frac{1 + r_1(t_0) z(q^2, t_0)}{1 + r_1(t_0) z(0, t_0)}, \quad (11)$$

where $t_0 = t_+(1 - \sqrt{1 - t_-/t_+})$, $t_\pm = (m_{D_s^+} \pm m_{K^0})^2$, and the functions $P(q^2)$, $\Phi(q^2, t_0)$, and $z(q^2, t_0)$ are defined following Ref. [33].

The statistical covariance matrix is constructed as

$$C^{\rm stat}_{ij} = \left(\frac{1}{\tau_{D_s^+} \cdot N^{\rm tot}_{\rm ST}}\right)^2 \sum_n \varepsilon^{-1}_{in} \varepsilon^{-1}_{jn} (\sigma(N^n_{\rm obs}))^2, \quad (12)$$

where n labels the q^2 interval and the sum extends from 1 to 5. The systematic covariance matrix is obtained by

TABLE V. Partial decay rates of $D_s^+ \to K^0 e^+ \nu_e$ in various q^2 intervals of data, where the uncertainties are statistical only.

q^2 interval	(0.0, 0.35]	(0.35, 0.70]	(0.70, 1.05]	(1.05, 1.40]	(1.40, 2.16]
$N^j_{\rm observed}$	60.7 ± 8.7	50.8 ± 8.1	46.1 ± 7.8	40.0 ± 6.7	30.2 ± 6.5
$N^i_{\rm produced}$	221.1 ± 32.5	172.2 ± 29.4	169.9 ± 28.9	146.2 ± 26.5	114.1 ± 25.4
$\Delta\Gamma_i$ (ns^{-1})	1.62 ± 0.24	1.26 ± 0.22	1.18 ± 0.21	1.07 ± 0.19	0.84 ± 0.19
$\frac{\Delta\Gamma_i}{\Delta q^2_i}$ (ns^{-1} GeV^{-2} c^4)	4.63 ± 0.68	3.60 ± 0.62	3.37 ± 0.60	3.06 ± 0.55	1.10 ± 0.24

TABLE VIII. Hadronic form factors of $D_s^+ \to K^0 e^+ \nu_e$, where the first uncertainties are statistical and the second systematic. The parameter for the two-parameter z series expansion is r_1 and the coefficient between the two fitted parameters is given in the fourth column. The χ^2/n.d.o.f. is the goodness of fit and n.d.o.f. is the number of degrees of freedom.

Parametrization	$f_+^{K^0}(0)\lvert V_{cd}\rvert$	Parameter ($M^2_{\rm pole}/\alpha/r_1$)	Coefficient	χ^2/n.d.o.f.	$f_+^{K^0}(0)$
Simple pole [32]	$0.147 \pm 0.009 \pm 0.001$	$1.75 \pm 0.09 \pm 0.03$	0.72	0.96/3	$0.654 \pm 0.040 \pm 0.004$
Modified pole [32]	$0.144 \pm 0.010 \pm 0.002$	$0.57 \pm 0.25 \pm 0.08$	−0.81	0.93/3	$0.640 \pm 0.044 \pm 0.009$
z series (two par.) [33]	$0.143 \pm 0.011 \pm 0.003$	$-3.7 \pm 1.5 \pm 0.5$	0.85	0.97/3	$0.636 \pm 0.049 \pm 0.013$

summing over the covariance matrix of each systematic uncertainty source. This is taken as

$$C_{ij}^{\rm syst} = \delta(\Delta\Gamma^i_{\rm measured})\delta(\Delta\Gamma^j_{\rm measured}), \tag{13}$$

where $\delta(\Delta\Gamma^i_{\rm measured})$ is the systematic uncertainty of the partial decay rate in the ith q^2 interval. The systematic uncertainties due to $\tau_{D_s^+}$, $N_{\rm ST}^{\rm tot}$, e^+ tracking efficiency, e^+ PID efficiency, K_S^0 reconstruction efficiency, transition γ reconstruction, $E^{\rm max}_{{\rm extra}\gamma}$ and $N^{\rm charge}_{\rm extra}$ requirements, $\chi^2_{\rm KMFIT}$ requirement, tag bias and quoted branching fraction are taken to be common across all the q^2 intervals. The systematic uncertainties due to $M^2_{\rm miss}$ fit, MC statistics, and hadronic form factor are determined separately in various q^2 intervals. The total systematic uncertainties of the measured partial decay rates in q^2 intervals from 1 to 5 are evaluated to be 3.93%, 4.00%, 4.51%, 3.84%, and 6.03%, respectively. The resulting statistical and systematic correlation coefficients are summarized in Tables VI and VII, respectively.

Minimizing the χ^2 constructed in Eq. (8), we obtain the product, $f_+^{K^0}(0)|V_{cd}|$, and the parameters of various hadronic form factor parametrizations. The obtained results are summarized in Table VIII and the fit results are shown in Fig. 5. The nominal fit parameters are taken from the fit with the combined statistical and systematic covariance matrix, and their statistical uncertainties are taken from the fit with the statistical covariance matrix. For each parameter, the systematic uncertainty is obtained by calculating the quadratic difference of uncertainties between these two fits. Taking the CKM matrix element $|V_{cd}| = 0.22486 \pm 0.00067$ [2] as input, we obtain $f_+^{K^0}(0)$ as summarized in the last column of Table VIII, where the first uncertainties are statistical and the second are systematic.

VIII. SUMMARY

In summary, using 7.33 fb^{-1} of e^+e^- collision data taken between 4.128 and 4.226 GeV with the BESIII detector, the branching fraction of $D_s^+ \to K^0 e^+ \nu_e$ is measured to be $(2.98 \pm 0.23 \pm 0.12) \times 10^{-3}$, where the first uncertainty is statistical and the second is the systematic. To measure the hadronic form factor at maximum recoil in $D_s^+ \to K^0 e^+ \nu_e$, we use the two parameter z series expansion. Based on fit to partial decay rates in various q^2 intervals, we measure $f_+^{K^0}(0)|V_{cd}| = 0.143 \pm 0.011 \pm 0.003$, and $f_+^{K^0}(0) = 0.636 \pm 0.049 \pm 0.013$ with $|V_{cd}| = 0.22486 \pm 0.00067$ [2] as an input. Figure 6 compares the measured branching fraction and the hadronic form factor in $D_s^+ \to K^0 e^+ \nu_e$ with theoretical calculations and other experiments. The precision of the measurements are improved by factors of 1.6 and 1.7, respectively, compared to the previous BESIII result [14]. The results can test various theoretical calculations.

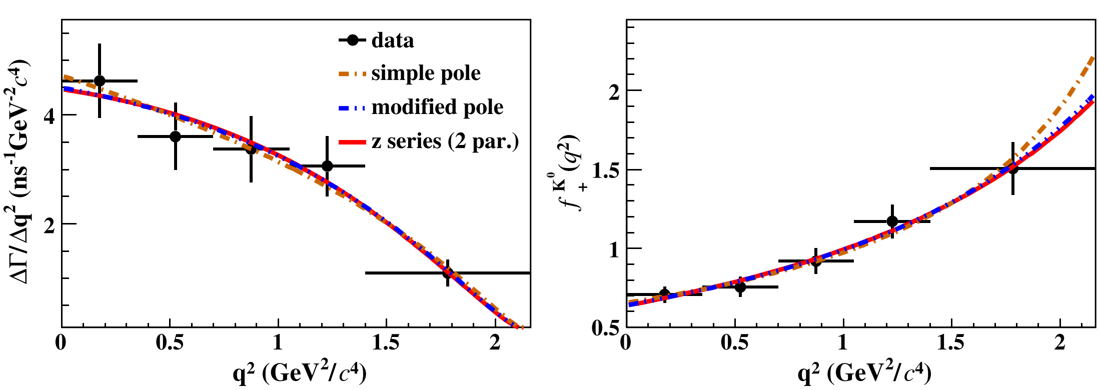

FIG. 5. Left: fit to the partial decay rates of $D_s^+ \to K^0 e^+ \nu_e$. Right: projection to the hadronic form factor as a function of q^2. The points with error bars are the measured partial decay rates, where the horizontal and vertical errors represent the q^2 bin interval and the error of the corresponding partial decay width, respectively. The solid red curves are the best fits.

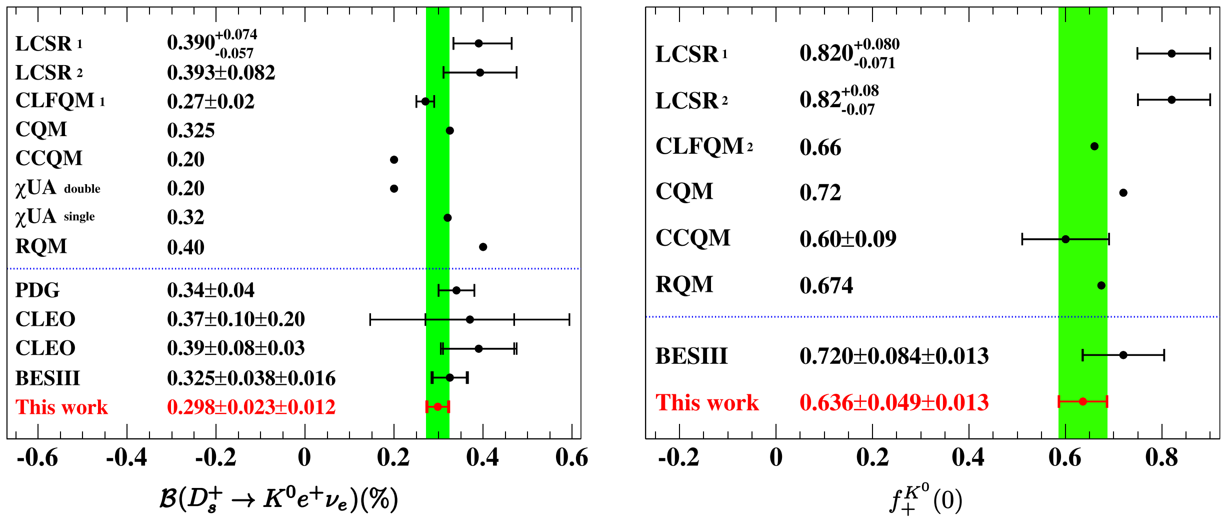

FIG. 6. Comparison of the measured branching fraction of $D_s^+ \to K^0 e^+ \nu_e$ (left) and the hadronic form factor (right) of $D_s^+ \to K^0$ with theoretical calculations and other experiments, where the bands show uncertainties of this measurements. The data in the comparison come from LCSR_1 [3], LCSR_2 [4], CLFQM_1 [5], CLFQM_2 [6], CQM [7], CCQM [8,9], $\chi^{\mathrm{UA}_{\text{double pole}}}$ [10], $\chi^{\mathrm{UA}_{\text{single pole}}}$ [10], RQM [11], PDG [2], CLEO [12], CLEO [13], and BESIII [14].

ACKNOWLEDGMENTS

The BESIII Collaboration thanks the staff of BEPCII and the IHEP computing center for their strong support. This work is supported in part by National Key R&D Program of China under Contracts No. 2020YFA0406400, No. 2023YFA1606000, No. 2020YFA0406300; National Natural Science Foundation of China (NSFC) under Contracts No. 11635010, No. 11735014, No. 11935015, No. 11935016, No. 11935018, No. 12022510, No. 12025502, No. 12035009, No. 12035013, No. 12061131003, No. 12192260, No. 12192261, No. 12192262, No. 12192263, No. 12192264, No. 12192265, No. 12221005, No. 12225509, No. 12235017, No. 12361141819, No. 12375090; the Chinese Academy of Sciences (CAS) Large-Scale Scientific Facility Program; the CAS Center for Excellence in Particle Physics (CCEPP); Joint Large-Scale Scientific Facility Funds of the NSFC and CAS under Contract No. U1832207; 100 Talents Program of CAS; The Institute of Nuclear and Particle Physics (INPAC) and Shanghai Key Laboratory for Particle Physics and Cosmology; German Research Foundation DFG under Contracts No. 455635585, No. FOR5327, GRK 2149; Istituto Nazionale di Fisica Nucleare, Italy; Knut and Alice Wallenberg Foundation under Contracts No. 2021.0174, No. 2021.0299; Ministry of Development of Turkey under Contract No. DPT2006K-120470; National Research Foundation of Korea under Contract No. NRF-2022R1A2C1092335; National Science and Technology fund of Mongolia; National Science Research and Innovation Fund (NSRF) via the Program Management Unit for Human Resources & Institutional Development, Research and Innovation of Thailand under Contract No. B16F640076; Polish National Science Centre under Contract No. 2019/35/O/ST2/02907; The Swedish Research Council; U.S. Department of Energy under Contract No. DE-FG02-05ER41374. This paper is also supported by the Fundamental Research Funds for the Central Universities, and the Research Funds of Renmin University of China under Contract No. 24XNKJ05.

[1] H. B. Li and X. R. Lyu, Natl. Sci. Rev. **8**, nwab181 (2021).
[2] R. L. Workman *et al.* (Particle Data Group), Prog. Theor. Exp. Phys. **2022**, 083C01 (2022).
[3] Y. L. Wu, M. Zhong, and Y. B. Zuo, Int. J. Mod. Phys. A **21**, 6125 (2006).
[4] X. Leng, X. L. Mu, Z. T. Zou, and Ying Li, Chin. Phys. C **45**, 063107 (2021).
[5] H. Y. Cheng and X. W. Kang, Eur. Phys. J. C **77**, 587 (2017); **77**, 863(E) (2017).
[6] R. C. Verma, J. Phys. G **39**, 025005 (2012).
[7] D. Melikhov and B. Stech, Phys. Rev. D **62**, 014006 (2000).
[8] N. R. Soni, M. A. Ivanov, J. G. Körner, J. N. Pandya, P. Santorelli, and C. T. Tran, Phys. Rev. D **98**, 114031 (2018).

[9] M. A. Ivanov, J. G. Körner, J. N. Pandya, P. Santorelli, N. R. Soni, and C. T. Tran, Front. Phys. (Beijing) **14**, 64401 (2019).
[10] S. Fajfer and J. Kamenik, Phys. Rev. D **71**, 014020 (2005).
[11] R. N. Faustov, V. O. Galkin, and X. W. Kang, Phys. Rev. D **101**, 013004 (2020).
[12] J. Yelton *et al.* (CLEO Collaboration), Phys. Rev. D **80**, 052007 (2009).
[13] J. Hietala, D. Cronin-Hennessy, T. Pedlar, and I. Shipsey, Phys. Rev. D **92**, 012009 (2015).
[14] M. Ablikim *et al.* (BESIII Collaboration), Phys. Rev. Lett. **122**, 061801 (2019).
[15] B. C. Ke, J. Koponen, H. B. Li, and Y. Zheng, Annu. Rev. Nucl. Part. Sci. **73**, 285 (2023).
[16] M. Ablikim *et al.* (BESIII Collaboration), Nucl. Instrum. Methods Phys. Res., Sect. A **614**, 345 (2010).
[17] C. H. Yu *et al.*, *Proceedings of IPAC2016, Busan, Korea* (JACoW, Geneva, Switzerland, 2016), 10.18429/JACoW-IPAC2016-TUYA01.
[18] M. Ablikim *et al.* (BESIII Collaboration), Chin. Phys. C **44**, 040001 (2020).
[19] X. Li *et al.*, Radiat. Detect. Technol. Methods **1**, 13 (2017); Y. X. Guo *et al.*, Radiat. Detect. Technol. Methods **1**, 15 (2017); P. Cao *et al.*, Nucl. Instrum. Methods Phys. Res., Sect. A **953**, 163053 (2020).
[20] S. Agostinelli *et al.* (GEANT4 Collaboration), Nucl. Instrum. Methods Phys. Res., Sect. A **506**, 250 (2003).
[21] S. Jadach, B. F. L. Ward, and Z. Was, Phys. Rev. D **63**, 113009 (2001); Comput. Phys. Commun. **130**, 260 (2000).
[22] R. G. Ping, Chin. Phys. C **38**, 083001 (2014).
[23] D. J. Lange, Nucl. Instrum. Methods Phys. Res., Sect. A **462**, 152 (2001); R. G. Ping, Chin. Phys. C **32**, 599 (2008).
[24] J. C. Chen, G. S. Huang, X. R. Qi, D. H. Zhang, and Y. S. Zhu, Phys. Rev. D **62**, 034003 (2000); R. L. Yang, R. G. Ping, and H. Chen, Chin. Phys. Lett. **31**, 061301 (2014).
[25] E. Richter-Was, Phys. Lett. B **303**, 163 (1993).
[26] R. M. Baltrusaitis *et al.* (MARK III Collaboration), Phys. Rev. Lett. **56**, 2140 (1986); **60**, 89 (1988).
[27] M. Ablikim *et al.* (BESIII Collaboration), Phys. Rev. Lett. **122**, 121801 (2019).
[28] M. Ablikim *et al.* (BESIII Collaboration), Phys. Rev. D **99**, 072002 (2019).
[29] M. Ablikim *et al.* (BESIII Collaboration), Phys. Rev. D **108**, 092003 (2023).
[30] M. Ablikim *et al.* (BESIII Collaboration), Phys. Rev. D **92**, 112008 (2015).
[31] M. Ablikim *et al.* (BESIII Collaboration), Phys. Rev. D **83**, 112005 (2011).
[32] D. Becirevcic and A. B. Kaidalov, Phys. Lett. B **478**, 417 (2000).
[33] T. Becher and R. J. Hill, Phys. Lett. B **633**, 61 (2006).

M. Ablikim,[1] M. N. Achasov,[4,c] P. Adlarson,[76] O. Afedulidis,[3] X. C. Ai,[81] R. Aliberti,[35] A. Amoroso,[75a,75c] Q. An,[72,58,a] Y. Bai,[57] O. Bakina,[36] I. Balossino,[29a] Y. Ban,[46,h] H.-R. Bao,[64] V. Batozskaya,[1,44] K. Begzsuren,[32] N. Berger,[35] M. Berlowski,[44] M. Bertani,[28a] D. Bettoni,[29a] F. Bianchi,[75a,75c] E. Bianco,[75a,75c] A. Bortone,[75a,75c] I. Boyko,[36] R. A. Briere,[5] A. Brueggemann,[69] H. Cai,[77] X. Cai,[1,58] A. Calcaterra,[28a] G. F. Cao,[1,64] N. Cao,[1,64] S. A. Cetin,[62a] J. F. Chang,[1,58] G. R. Che,[43] G. Chelkov,[36,b] C. Chen,[43] C. H. Chen,[9] Chao Chen,[55] G. Chen,[1] H. S. Chen,[1,64] H. Y. Chen,[20] M. L. Chen,[1,58,64] S. J. Chen,[42] S. L. Chen,[45] S. M. Chen,[61] T. Chen,[1,64] X. R. Chen,[31,64] X. T. Chen,[1,64] Y. B. Chen,[1,58] Y. Q. Chen,[34] Z. J. Chen,[25,i] Z. Y. Chen,[1,64] S. K. Choi,[10] G. Cibinetto,[29a] F. Cossio,[75c] J. J. Cui,[50] H. L. Dai,[1,58] J. P. Dai,[79] A. Dbeyssi,[18] R. E. de Boer,[3] D. Dedovich,[36] C. Q. Deng,[73] Z. Y. Deng,[1] A. Denig,[35] I. Denysenko,[36] M. Destefanis,[75a,75c] F. De Mori,[75a,75c] B. Ding,[67,1] X. X. Ding,[46,h] Y. Ding,[34] Y. Ding,[40] J. Dong,[1,58] L. Y. Dong,[1,64] M. Y. Dong,[1,58,64] X. Dong,[77] M. C. Du,[1] S. X. Du,[81] Y. Y. Duan,[55] Z. H. Duan,[42] P. Egorov,[36,b] Y. H. Fan,[45] J. Fang,[59] J. Fang,[1,58] S. S. Fang,[1,64] W. X. Fang,[1] Y. Fang,[1] Y. Q. Fang,[1,58] R. Farinelli,[29a] L. Fava,[75b,75c] F. Feldbauer,[3] G. Felici,[28a] C. Q. Feng,[72,58] J. H. Feng,[59] Y. T. Feng,[72,58] M. Fritsch,[3] C. D. Fu,[1] J. L. Fu,[64] Y. W. Fu,[1,64] H. Gao,[64] X. B. Gao,[41] Y. N. Gao,[46,h] Yang Gao,[72,58] S. Garbolino,[75c] I. Garzia,[29a,29b] L. Ge,[81] P. T. Ge,[19] Z. W. Ge,[42] C. Geng,[59] E. M. Gersabeck,[68] A. Gilman,[70] K. Goetzen,[13] L. Gong,[40] W. X. Gong,[1,58] W. Gradl,[35] S. Gramigna,[29a,29b] M. Greco,[75a,75c] M. H. Gu,[1,58] Y. T. Gu,[15] C. Y. Guan,[1,64] A. Q. Guo,[31,64] L. B. Guo,[41] M. J. Guo,[50] R. P. Guo,[49] Y. P. Guo,[12,g] A. Guskov,[36,b] J. Gutierrez,[27] K. L. Han,[64] T. T. Han,[1] F. Hanisch,[3] X. Q. Hao,[19] F. A. Harris,[66] K. K. He,[55] K. L. He,[1,64] F. H. Heinsius,[3] C. H. Heinz,[35] Y. K. Heng,[1,58,64] C. Herold,[60] T. Holtmann,[3] P. C. Hong,[34] G. Y. Hou,[1,64] X. T. Hou,[1,64] Y. R. Hou,[64] Z. L. Hou,[1] B. Y. Hu,[59] H. M. Hu,[1,64] J. F. Hu,[56,j] S. L. Hu,[12,g] T. Hu,[1,58,64] Y. Hu,[1] G. S. Huang,[72,58] K. X. Huang,[59] L. Q. Huang,[31,64] X. T. Huang,[50] Y. P. Huang,[1] Y. S. Huang,[59] T. Hussain,[74] F. Hölzken,[3] N. Hüsken,[35] N. in der Wiesche,[69] J. Jackson,[27] S. Janchiv,[32] J. H. Jeong,[10] Q. Ji,[1] Q. P. Ji,[19] W. Ji,[1,64] X. B. Ji,[1,64] X. L. Ji,[1,58] Y. Y. Ji,[50] X. Q. Jia,[50] Z. K. Jia,[72,58] D. Jiang,[1,64] H. B. Jiang,[77] P. C. Jiang,[46,h] S. S. Jiang,[39] T. J. Jiang,[16] X. S. Jiang,[1,58,64] Y. Jiang,[64] J. B. Jiao,[50] J. K. Jiao,[34] Z. Jiao,[23] S. Jin,[42] Y. Jin,[67] M. Q. Jing,[1,64] X. M. Jing,[64] T. Johansson,[76] S. Kabana,[33] N. Kalantar-Nayestanaki,[65] X. L. Kang,[9] X. S. Kang,[40] M. Kavatsyuk,[65] B. C. Ke,[81] V. Khachatryan,[27] A. Khoukaz,[69] R. Kiuchi,[1] O. B. Kolcu,[62a] B. Kopf,[3] M. Kuessner,[3] X. Kui,[1,64] N. Kumar,[26] A. Kupsc,[44,76] W. Kühn,[37] J. J. Lane,[68] L. Lavezzi,[75a,75c] T. T. Lei,[72,58] Z. H. Lei,[72,58] M. Lellmann,[35] T. Lenz,[35] C. Li,[47]

C. Li,[43] C. H. Li,[39] Cheng Li,[72,58] D. M. Li,[81] F. Li,[1,58] G. Li,[1] H. B. Li,[1,64] H. J. Li,[19] H. N. Li,[56,j] Hui Li,[43] J. R. Li,[61] J. S. Li,[59] K. Li,[1] L. J. Li,[1,64] L. K. Li,[1] Lei Li,[48] M. H. Li,[43] P. R. Li,[38,k,l] Q. M. Li,[1,64] Q. X. Li,[50] R. Li,[17,31] S. X. Li,[12] T. Li,[50] W. D. Li,[1,64] W. G. Li,[1,a] X. Li,[1,64] X. H. Li,[72,58] X. L. Li,[50] X. Y. Li,[1,64] X. Z. Li,[59] Y. G. Li,[46,h] Z. J. Li,[59] Z. Y. Li,[79] C. Liang,[42] H. Liang,[72,58] H. Liang,[1,64] Y. F. Liang,[54] Y. T. Liang,[31,64] G. R. Liao,[14] Y. P. Liao,[1,64] J. Libby,[26] A. Limphirat,[60] C. C. Lin,[55] D. X. Lin,[31,64] T. Lin,[1] B. J. Liu,[1] B. X. Liu,[77] C. Liu,[34] C. X. Liu,[1] F. Liu,[1] F. H. Liu,[53] Feng Liu,[6] G. M. Liu,[56,j] H. Liu,[38,k,l] H. B. Liu,[15] H. H. Liu,[1] H. M. Liu,[1,64] Huihui Liu,[21] J. B. Liu,[72,58] J. Y. Liu,[1,64] K. Liu,[38,k,l] K. Y. Liu,[40] Ke Liu,[22] L. Liu,[72,58] L. C. Liu,[43] Lu Liu,[43] M. H. Liu,[12,g] N. Liu,[47] P. L. Liu,[1] Q. Liu,[64] S. B. Liu,[72,58] T. Liu,[12,g] W. K. Liu,[43] W. M. Liu,[72,58] X. Liu,[38,k,l] X. Liu,[39] Y. Liu,[38,k,l] Y. Liu,[81] Y. B. Liu,[43] Z. A. Liu,[1,58,64] Z. D. Liu,[9] Z. Q. Liu,[50] X. C. Lou,[1,58,64] F. X. Lu,[59] H. J. Lu,[23] J. G. Lu,[1,58] X. L. Lu,[1] Y. Lu,[7] Y. P. Lu,[1,58] Z. H. Lu,[1,64] C. L. Luo,[41] J. R. Luo,[59] M. X. Luo,[80] T. Luo,[12,g] X. L. Luo,[1,58] X. R. Lyu,[64] Y. F. Lyu,[43] F. C. Ma,[40] H. Ma,[79] H. L. Ma,[1] J. L. Ma,[1,64] L. L. Ma,[50] L. R. Ma,[67] M. M. Ma,[1,64] Q. M. Ma,[1] R. Q. Ma,[1,64] T. Ma,[72,58] X. T. Ma,[1,64] X. Y. Ma,[1,58] Y. Ma,[46,h] Y. M. Ma,[31] F. E. Maas,[18] M. Maggiora,[75a,75c] S. Malde,[70] Y. J. Mao,[46,h] Z. P. Mao,[1] S. Marcello,[75a,75c] Z. X. Meng,[67] J. G. Messchendorp,[13,65] G. Mezzadri,[29a] H. Miao,[1,64] T. J. Min,[42] R. E. Mitchell,[27] X. H. Mo,[1,58,64] B. Moses,[27] N. Yu. Muchnoi,[4,c] J. Muskalla,[35] Y. Nefedov,[36] F. Nerling,[18,e] L. S. Nie,[20] I. B. Nikolaev,[4,c] Z. Ning,[1,58] S. Nisar,[11,m] Q. L. Niu,[38,k,l] W. D. Niu,[55] Y. Niu,[50] S. L. Olsen,[64] Q. Ouyang,[1,58,64] S. Pacetti,[28b,28c] X. Pan,[55] Y. Pan,[57] A. Pathak,[34] Y. P. Pei,[72,58] M. Pelizaeus,[3] H. P. Peng,[72,58] Y. Y. Peng,[38,k,l] K. Peters,[13,e] J. L. Ping,[41] R. G. Ping,[1,64] S. Plura,[35] V. Prasad,[33] F. Z. Qi,[1] H. Qi,[72,58] H. R. Qi,[61] M. Qi,[42] T. Y. Qi,[12,g] S. Qian,[1,58] W. B. Qian,[64] C. F. Qiao,[64] X. K. Qiao,[81] J. J. Qin,[73] L. Q. Qin,[14] L. Y. Qin,[72,58] X. P. Qin,[12,g] X. S. Qin,[50] Z. H. Qin,[1,58] J. F. Qiu,[1] Z. H. Qu,[73] C. F. Redmer,[35] K. J. Ren,[39] A. Rivetti,[75c] M. Rolo,[75c] G. Rong,[1,64] Ch. Rosner,[18] S. N. Ruan,[43] N. Salone,[44] A. Sarantsev,[36,d] Y. Schelhaas,[35] K. Schoenning,[76] M. Scodeggio,[29a] K. Y. Shan,[12,g] W. Shan,[24] X. Y. Shan,[72,58] Z. J. Shang,[38,k,l] J. F. Shangguan,[16] L. G. Shao,[1,64] M. Shao,[72,58] C. P. Shen,[12,g] H. F. Shen,[1,8] W. H. Shen,[64] X. Y. Shen,[1,64] B. A. Shi,[64] H. Shi,[72,58] H. C. Shi,[72,58] J. L. Shi,[12,g] J. Y. Shi,[1] Q. Q. Shi,[55] S. Y. Shi,[73] X. Shi,[1,58] J. J. Song,[19] T. Z. Song,[59] W. M. Song,[34,1] Y. J. Song,[12,g] Y. X. Song,[46,h,n] S. Sosio,[75a,75c] S. Spataro,[75a,75c] F. Stieler,[35] S. S. Su,[40] Y. J. Su,[64] G. B. Sun,[77] G. X. Sun,[1] H. Sun,[64] H. K. Sun,[1] J. F. Sun,[19] K. Sun,[61] L. Sun,[77] S. S. Sun,[1,64] T. Sun,[51,f] W. Y. Sun,[34] Y. Sun,[9] Y. J. Sun,[72,58] Y. Z. Sun,[1] Z. Q. Sun,[1,64] Z. T. Sun,[50] C. J. Tang,[54] G. Y. Tang,[1] J. Tang,[59] M. Tang,[72,58] Y. A. Tang,[77] L. Y. Tao,[73] Q. T. Tao,[25,i] M. Tat,[70] J. X. Teng,[72,58] V. Thoren,[76] W. H. Tian,[59] Y. Tian,[31,64] Z. F. Tian,[77] I. Uman,[62b] Y. Wan,[55] S. J. Wang,[50] B. Wang,[1] B. L. Wang,[64] Bo Wang,[72,58] D. Y. Wang,[46,h] F. Wang,[73] H. J. Wang,[38,k,l] J. J. Wang,[77] J. P. Wang,[50] K. Wang,[1,58] L. L. Wang,[1] M. Wang,[50] N. Y. Wang,[64] S. Wang,[38,k,l] S. Wang,[12,g] T. Wang,[12,g] T. J. Wang,[43] W. Wang,[59] W. Wang,[73] W. P. Wang,[35,72,o] X. Wang,[46,h] X. F. Wang,[38,k,l] X. J. Wang,[39] X. L. Wang,[12,g] X. N. Wang,[1] Y. Wang,[61] Y. D. Wang,[45] Y. F. Wang,[1,58,64] Y. L. Wang,[19] Y. N. Wang,[45] Y. Q. Wang,[1] Yaqian Wang,[17] Yi Wang,[61] Z. Wang,[1,58] Z. L. Wang,[73] Z. Y. Wang,[1,64] Ziyi Wang,[64] D. H. Wei,[14] F. Weidner,[69] S. P. Wen,[1] Y. R. Wen,[39] U. Wiedner,[3] G. Wilkinson,[70] M. Wolke,[76] L. Wollenberg,[3] C. Wu,[39] J. F. Wu,[1,8] L. H. Wu,[1] L. J. Wu,[1,64] X. Wu,[12,g] X. H. Wu,[34] Y. Wu,[72,58] Y. H. Wu,[55] Y. J. Wu,[31] Z. Wu,[1,58] L. Xia,[72,58] X. M. Xian,[39] B. H. Xiang,[1,64] T. Xiang,[46,h] D. Xiao,[38,k,l] G. Y. Xiao,[42] S. Y. Xiao,[1] Y. L. Xiao,[12,g] Z. J. Xiao,[41] C. Xie,[42] X. H. Xie,[46,h] Y. Xie,[50] Y. G. Xie,[1,58] Y. H. Xie,[6] Z. P. Xie,[72,58] T. Y. Xing,[1,64] C. F. Xu,[1,64] C. J. Xu,[59] G. F. Xu,[1] H. Y. Xu,[67,2,p] M. Xu,[72,58] Q. J. Xu,[16] Q. N. Xu,[30] W. Xu,[1] W. L. Xu,[67] X. P. Xu,[55] Y. Xu,[40] Y. C. Xu,[78] Z. S. Xu,[64] F. Yan,[12,g] L. Yan,[12,g] W. B. Yan,[72,58] W. C. Yan,[81] X. Q. Yan,[1,64] H. J. Yang,[51,f] H. L. Yang,[34] H. X. Yang,[1] T. Yang,[1] Y. Yang,[12,g] Y. F. Yang,[1,64] Y. F. Yang,[43] Y. X. Yang,[1,64] Z. W. Yang,[38,k,l] Z. P. Yao,[50] M. Ye,[1,58] M. H. Ye,[8] J. H. Yin,[1] Junhao Yin,[43] Z. Y. You,[59] B. X. Yu,[1,58,64] C. X. Yu,[43] G. Yu,[1,64] J. S. Yu,[25,i] M. C. Yu,[40] T. Yu,[73] X. D. Yu,[46,h] Y. C. Yu,[81] C. Z. Yuan,[1,64] J. Yuan,[34] J. Yuan,[45] L. Yuan,[2] S. C. Yuan,[1,64] Y. Yuan,[1,64] Z. Y. Yuan,[59] C. X. Yue,[39] A. A. Zafar,[74] F. R. Zeng,[50] S. H. Zeng,[63] X. Zeng,[12,g] Y. Zeng,[25,i] Y. J. Zeng,[1,64] Y. J. Zeng,[59] X. Y. Zhai,[34] Y. C. Zhai,[50] Y. H. Zhan,[59] A. Q. Zhang,[1,64] B. L. Zhang,[1,64] B. X. Zhang,[1] D. H. Zhang,[43] G. Y. Zhang,[19] H. Zhang,[81] H. Zhang,[72,58] H. C. Zhang,[1,58,64] H. H. Zhang,[34] H. H. Zhang,[59] H. Q. Zhang,[1,58,64] H. R. Zhang,[72,58] H. Y. Zhang,[1,58] J. Zhang,[81] J. Zhang,[59] J. J. Zhang,[52] J. L. Zhang,[20] J. Q. Zhang,[41] J. S. Zhang,[12,g] J. W. Zhang,[1,58,64] J. X. Zhang,[38,k,l] J. Y. Zhang,[1] J. Z. Zhang,[1,64] Jianyu Zhang,[64] L. M. Zhang,[61] Lei Zhang,[42] P. Zhang,[1,64] Q. Y. Zhang,[34] R. Y. Zhang,[38,k,l] S. H. Zhang,[1,64] Shulei Zhang,[25,i] X. D. Zhang,[45] X. M. Zhang,[1] X. Y. Zhang,[40] X. Y. Zhang,[50] Y. Zhang,[73] Y. Zhang,[1] Y. T. Zhang,[81] Y. H. Zhang,[1,58] Y. M. Zhang,[39] Yan Zhang,[72,58] Z. D. Zhang,[1] Z. H. Zhang,[1] Z. L. Zhang,[34] Z. Y. Zhang,[43] Z. Y. Zhang,[77] Z. Z. Zhang,[45] G. Zhao,[1] J. Y. Zhao,[1,64] J. Z. Zhao,[1,58] L. Zhao,[1] Lei Zhao,[72,58] M. G. Zhao,[43] N. Zhao,[79] R. P. Zhao,[64] S. J. Zhao,[81] Y. B. Zhao,[1,58] Y. X. Zhao,[31,64] Z. G. Zhao,[72,58] A. Zhemchugov,[36,b] B. Zheng,[73] B. M. Zheng,[34] J. P. Zheng,[1,58] W. J. Zheng,[1,64] Y. H. Zheng,[64] B. Zhong,[41] X. Zhong,[59] H. Zhou,[50] J. Y. Zhou,[34] L. P. Zhou,[1,64] S. Zhou,[6] X. Zhou,[77] X. K. Zhou,[6] X. R. Zhou,[72,58] X. Y. Zhou,[39] Y. Z. Zhou,[12,g] Z. C. Zhou,[20] A. N. Zhu,[64]

J. Zhu,[43] K. Zhu,[1] K. J. Zhu,[1,58,64] K. S. Zhu,[12,g] L. Zhu,[34] L. X. Zhu,[64] S. H. Zhu,[71] T. J. Zhu,[12,g] W. D. Zhu,[41] Y. C. Zhu,[72,58] Z. A. Zhu,[1,64] J. H. Zou,[1] and J. Zu[72,58]

(BESIII Collaboration)

[1]*Institute of High Energy Physics, Beijing 100049, People's Republic of China*
[2]*Beihang University, Beijing 100191, People's Republic of China*
[3]*Bochum Ruhr-University, D-44780 Bochum, Germany*
[4]*Budker Institute of Nuclear Physics SB RAS (BINP), Novosibirsk 630090, Russia*
[5]*Carnegie Mellon University, Pittsburgh, Pennsylvania 15213, USA*
[6]*Central China Normal University, Wuhan 430079, People's Republic of China*
[7]*Central South University, Changsha 410083, People's Republic of China*
[8]*China Center of Advanced Science and Technology, Beijing 100190, People's Republic of China*
[9]*China University of Geosciences, Wuhan 430074, People's Republic of China*
[10]*Chung-Ang University, Seoul, 06974, Republic of Korea*
[11]*COMSATS University Islamabad, Lahore Campus, Defence Road, Off Raiwind Road, 54000 Lahore, Pakistan*
[12]*Fudan University, Shanghai 200433, People's Republic of China*
[13]*GSI Helmholtzcentre for Heavy Ion Research GmbH, D-64291 Darmstadt, Germany*
[14]*Guangxi Normal University, Guilin 541004, People's Republic of China*
[15]*Guangxi University, Nanning 530004, People's Republic of China*
[16]*Hangzhou Normal University, Hangzhou 310036, People's Republic of China*
[17]*Hebei University, Baoding 071002, People's Republic of China*
[18]*Helmholtz Institute Mainz, Staudinger Weg 18, D-55099 Mainz, Germany*
[19]*Henan Normal University, Xinxiang 453007, People's Republic of China*
[20]*Henan University, Kaifeng 475004, People's Republic of China*
[21]*Henan University of Science and Technology, Luoyang 471003, People's Republic of China*
[22]*Henan University of Technology, Zhengzhou 450001, People's Republic of China*
[23]*Huangshan College, Huangshan 245000, People's Republic of China*
[24]*Hunan Normal University, Changsha 410081, People's Republic of China*
[25]*Hunan University, Changsha 410082, People's Republic of China*
[26]*Indian Institute of Technology Madras, Chennai 600036, India*
[27]*Indiana University, Bloomington, Indiana 47405, USA*
[28a]*INFN Laboratori Nazionali di Frascati, I-00044, Frascati, Italy*
[28b]*INFN Laboratori Nazionali di Frascati, INFN Sezione di Perugia, I-06100, Perugia, Italy*
[28c]*INFN Laboratori Nazionali di Frascati, University of Perugia, I-06100, Perugia, Italy*
[29a]*INFN Sezione di Ferrara, I-44122, Ferrara, Italy*
[29b]*INFN Sezione di Ferrara, University of Ferrara, I-44122, Ferrara, Italy*
[30]*Inner Mongolia University, Hohhot 010021, People's Republic of China*
[31]*Institute of Modern Physics, Lanzhou 730000, People's Republic of China*
[32]*Institute of Physics and Technology, Peace Avenue 54B, Ulaanbaatar 13330, Mongolia*
[33]*Instituto de Alta Investigación, Universidad de Tarapacá, Casilla 7D, Arica 1000000, Chile*
[34]*Jilin University, Changchun 130012, People's Republic of China*
[35]*Johannes Gutenberg University of Mainz, Johann-Joachim-Becher-Weg 45, D-55099 Mainz, Germany*
[36]*Joint Institute for Nuclear Research, 141980 Dubna, Moscow region, Russia*
[37]*Justus-Liebig-Universitaet Giessen, II. Physikalisches Institut, Heinrich-Buff-Ring 16, D-35392 Giessen, Germany*
[38]*Lanzhou University, Lanzhou 730000, People's Republic of China*
[39]*Liaoning Normal University, Dalian 116029, People's Republic of China*
[40]*Liaoning University, Shenyang 110036, People's Republic of China*
[41]*Nanjing Normal University, Nanjing 210023, People's Republic of China*
[42]*Nanjing University, Nanjing 210093, People's Republic of China*
[43]*Nankai University, Tianjin 300071, People's Republic of China*
[44]*National Centre for Nuclear Research, Warsaw 02-093, Poland*
[45]*North China Electric Power University, Beijing 102206, People's Republic of China*
[46]*Peking University, Beijing 100871, People's Republic of China*
[47]*Qufu Normal University, Qufu 273165, People's Republic of China*
[48]*Renmin University of China, Beijing 100872, People's Republic of China*
[49]*Shandong Normal University, Jinan 250014, People's Republic of China*

[50]*Shandong University, Jinan 250100, People's Republic of China*
[51]*Shanghai Jiao Tong University, Shanghai 200240, People's Republic of China*
[52]*Shanxi Normal University, Linfen 041004, People's Republic of China*
[53]*Shanxi University, Taiyuan 030006, People's Republic of China*
[54]*Sichuan University, Chengdu 610064, People's Republic of China*
[55]*Soochow University, Suzhou 215006, People's Republic of China*
[56]*South China Normal University, Guangzhou 510006, People's Republic of China*
[57]*Southeast University, Nanjing 211100, People's Republic of China*
[58]*State Key Laboratory of Particle Detection and Electronics, Beijing 100049, Hefei 230026, People's Republic of China*
[59]*Sun Yat-Sen University, Guangzhou 510275, People's Republic of China*
[60]*Suranaree University of Technology, University Avenue 111, Nakhon Ratchasima 30000, Thailand*
[61]*Tsinghua University, Beijing 100084, People's Republic of China*
[62a]*Turkish Accelerator Center Particle Factory Group, Istinye University, 34010, Istanbul, Turkey*
[62b]*Turkish Accelerator Center Particle Factory Group, Near East University, Nicosia, North Cyprus, 99138, Mersin 10, Turkey*
[63]*University of Bristol, H H Wills Physics Laboratory, Tyndall Avenue, Bristol BS8 1TL, United Kingdom*
[64]*University of Chinese Academy of Sciences, Beijing 100049, People's Republic of China*
[65]*University of Groningen, NL-9747 AA Groningen, The Netherlands*
[66]*University of Hawaii, Honolulu, Hawaii 96822, USA*
[67]*University of Jinan, Jinan 250022, People's Republic of China*
[68]*University of Manchester, Oxford Road, Manchester M13 9PL, United Kingdom*
[69]*University of Muenster, Wilhelm-Klemm-Strasse 9, 48149 Muenster, Germany*
[70]*University of Oxford, Keble Road, Oxford OX13RH, United Kingdom*
[71]*University of Science and Technology Liaoning, Anshan 114051, People's Republic of China*
[72]*University of Science and Technology of China, Hefei 230026, People's Republic of China*
[73]*University of South China, Hengyang 421001, People's Republic of China*
[74]*University of the Punjab, Lahore-54590, Pakistan*
[75a]*University of Turin and INFN, University of Turin, I-10125, Turin, Italy*
[75b]*University of Turin and INFN, University of Eastern Piedmont, I-15121, Alessandria, Italy*
[75c]*University of Turin and INFN, INFN, I-10125, Turin, Italy*
[76]*Uppsala University, Box 516, SE-75120 Uppsala, Sweden*
[77]*Wuhan University, Wuhan 430072, People's Republic of China*
[78]*Yantai University, Yantai 264005, People's Republic of China*
[79]*Yunnan University, Kunming 650500, People's Republic of China*
[80]*Zhejiang University, Hangzhou 310027, People's Republic of China*
[81]*Zhengzhou University, Zhengzhou 450001, People's Republic of China*

[a]Deceased.
[b]Also at the Moscow Institute of Physics and Technology, Moscow 141700, Russia.
[c]Also at the Novosibirsk State University, Novosibirsk, 630090, Russia.
[d]Also at the NRC "Kurchatov Institute," PNPI, 188300, Gatchina, Russia.
[e]Also at Goethe University Frankfurt, 60323 Frankfurt am Main, Germany.
[f]Also at Key Laboratory for Particle Physics, Astrophysics and Cosmology, Ministry of Education; Shanghai Key Laboratory for Particle Physics and Cosmology; Institute of Nuclear and Particle Physics, Shanghai 200240, People's Republic of China.
[g]Also at Key Laboratory of Nuclear Physics and Ion-beam Application (MOE) and Institute of Modern Physics, Fudan University, Shanghai 200443, People's Republic of China.
[h]Also at State Key Laboratory of Nuclear Physics and Technology, Peking University, Beijing 100871, People's Republic of China.
[i]Also at School of Physics and Electronics, Hunan University, Changsha 410082, China.
[j]Also at Guangdong Provincial Key Laboratory of Nuclear Science, Institute of Quantum Matter, South China Normal University, Guangzhou 510006, China.
[k]Also at MOE Frontiers Science Center for Rare Isotopes, Lanzhou University, Lanzhou 730000, People's Republic of China.
[l]Also at Lanzhou Center for Theoretical Physics, Lanzhou University, Lanzhou 730000, People's Republic of China.
[m]Also at the Department of Mathematical Sciences, IBA, Karachi 75270, Pakistan.
[n]Also at Ecole Polytechnique Federale de Lausanne (EPFL), CH-1015 Lausanne, Switzerland.
[o]Also at Helmholtz Institute Mainz, Staudinger Weg 18, D-55099 Mainz, Germany.
[p]Also at School of Physics, Beihang University, Beijing 100191, China.